

Article

Data-Driven Deformation Prediction of Accumulation Landslides in the Middle Qinling-Bashan Mountains Area

Juan Ma ^{1,2,†}, Qiang Yang ^{2,*,†}, Mingzhi Zhang ^{2,3,*}, Yao Chen ⁴, Wenyi Zhao ^{1,2}, Chengyu Ouyang ⁵ and Dongping Ming ^{6,7} 

¹ School of Engineering and Technology, China University of Geosciences (Beijing), Beijing 100083, China; majuan@mail.cgs.gov.cn (J.M.)

² China Institute of Geo-Environment Monitoring, Beijing 100081, China

³ Department of Engineering Physics, Tsinghua University, Beijing 100084, China

⁴ Institute of Geological Survey, China University of Geosciences (Wuhan), Wuhan 430074, China

⁵ Wuhan Infoearth Information Engineering Co., Ltd, Wuhan 430074, China

⁶ School of Information Engineering, China University of Geosciences (Beijing), Beijing 100083, China

⁷ Frontiers Science Center for Deep-Time Digital Earth, China University of Geosciences (Beijing), Beijing 100083, China

* Correspondence: yang5359535@126.com (Q.Y.); zhangmz@cigem.cn (M.Z.); Tel.: +86-177-1002-8388 (Q.Y.); +86-138-1009-3685 (M.Z.)

† These authors contributed equally to this work.

Abstract: Accurately predicting landslide deformation based on monitoring data is key to successful early warning of landslide disasters. Landslide displacement–time curves offer an intuitive reflection of the landslide motion process and deformation predictions often reference the Saito curve for correlational analysis with cumulative deformation curves. Many scholars have applied machine learning techniques to individual landslide deformation predictions with considerable success. However, most landslide monitoring data lack a full lifecycle, making it challenging to predict unexperienced evolutionary stages. Cross-learning between similar landslide datasets provides a potential solution to issues of data scarcity and accurate prediction. First, this paper proposes a landslide classification and displacement machine learning method, along with predictive performance evaluation metrics. Further, it details a study of 13 landslides with evident deformation signs in the middle Qinling–Bashan Mountains area, conducting refined landslide classification. Based on a data-driven approach, this study conducts an analysis of the importance of characteristics influencing landslide deformation and establishes predictive models for similar-type landslide deformation, mixed-type landslide deformation, and individual landslide deformation using machine learning algorithms. The models trained on the dataset are used to predict the deformation of the West of Yinpo Yard landslide at different periods, with the predictive performance evaluated using two indices. The results indicate that the models trained on similar-type landslide data and those based on individual landslide data yielded comparable predictive performances, substantially addressing challenges such as insufficient early-stage monitoring data and low prediction accuracy.

Keywords: Qinling–Bashan Mountains; landslide; data-driven; machine learning; deformation prediction



Citation: Ma, J.; Yang, Q.; Zhang, M.; Chen, Y.; Zhao, W.; Ouyang, C.; Ming, D. Data-Driven Deformation Prediction of Accumulation Landslides in the Middle Qinling-Bashan Mountains Area. *Water* **2024**, *16*, 464. <https://doi.org/10.3390/w16030464>

Academic Editor: Yijun Xu

Received: 25 December 2023

Revised: 22 January 2024

Accepted: 22 January 2024

Published: 31 January 2024



Copyright: © 2024 by the authors. Licensee MDPI, Basel, Switzerland. This article is an open access article distributed under the terms and conditions of the Creative Commons Attribution (CC BY) license (<https://creativecommons.org/licenses/by/4.0/>).

1. Introduction

Due to the movements of the Pacific Plate, the Indian Ocean Plate and the Asian–European Plate, China is characterized by strong tectonic and seismic activities, and complex topography and geological conditions, coupled with a variety of climatic types and intense human engineering activities, which make geologic hazards prone to occurring, prolific, and frequent. The middle Qinling–Bashan Mountains area is an area highly prone to geologic hazards, and is located in the key prevention and control area of landslides, avalanches, and mudslides in the Qinling-Bashan Mountains of China. The geological disasters in the region are characterized as cluster, regional, and chain-born. The distribution

density of geologic hazard sites is three times higher than the average density in China. The study area is characterized by strong internal and external dynamics, active earthquakes, strong development of active fractures, deep ravines and valleys, large relative height difference in topography, relatively high rainfall, frequent human engineering activities, and frequent occurrence of geologic hazards such as avalanches, landslides, mudslides, and other geologic hazards, especially the stacked layer landslide disasters, which are extremely common, accounting for about 89.6% of the total [1,2].

Understanding how to effectively carry out the prediction of landslide deformation in the middle accumulation layer of the Qinling–Bashan Mountains area can help in grasping the deformation and destabilization process of landslides in this area, and reduce the risk of landslides to the safety of people's lives and property, and the safety of major projects. Many experts and scholars have carried out qualitative and quantitative studies on landslide displacement prediction with different methods, using empirical models, mathematical statistical models, nonlinear models, etc. for landslide prediction [3–7]. For example, Yin Shunde et al. [8] used the evolutionary neural network GA-NN model to make an accurate prediction of the evolutionary development of landslide displacements under rainfall conditions. Wang Chaoyang et al. [9] established a Grey System Metabolic GM(1,1) landslide prediction model to predict the displacement and deformation of the Xiangjiapo landslide and the GA monitoring point of the chain cliff hazardous rock body. Deng Dongmei et al. [10] proposed, for the displacement prediction work of reservoir level landslide fluctuation term in the Three Gorges reservoir area, the particle swarm optimization-support vector machine regression (PSO-SVR) displacement prediction method based on time-series ensemble empirical modal decomposition and reconstruction with the Baishui River landslide as the research object.

Researchers have implemented some advanced machine learning methods to predict landslide displacement, achieving high precision in forecasting and providing technical support for landslide risk assessment and early warning. However, shortcomings remain. Currently, most predictions of landslide displacement integrate inducing factors such as rainfall and reservoir water levels, along with long-term displacement data series. The accuracy of the predictions is closely related to the quality of historical data; predictions are more precise when historical data fully reflect the coupling relationship between the landslide evolution process and multiple influencing factors, and less precise otherwise [11–19]. Previous studies have not conducted comparative research on displacement datasets of similar landslides; they typically lack long-term, high-temporal-resolution complete deformation data. Furthermore, these studies usually apply machine learning models to individual landslides without extending the trained models to other sites, leading to inadequate validation of the models' generalizability.

This paper proposes a method for predicting similar-type landslide deformation and establishes a data-driven model, aiming to address challenges such as insufficient early-stage monitoring data and low prediction accuracy. The study selects 13 landslides in the middle Qinling–Bashan Mountains area, which exhibit significant deformation signs in the accumulation layer, as research subjects. Utilizing machine learning algorithms and combining rainfall and deformation monitoring data, the study conducts a comparative analysis of three types of predictive models: those for similar-type landslide deformation, mixed-type landslide deformation, and individual landslide prediction. Models trained on data from similar-type landslides are then applied to predict deformation in other landslides to evaluate the generalizability and applicability of the similar-type landslide deformation prediction model.

2. Methods

2.1. Classification of Landslides Method

Landslides are formed in different geological environments, and manifested in different forms and features; all types of landslides have their own development and evolution process and law, and there are significant differences in the sliding law presented by differ-

ent influencing factors. There are many existing classification standards for landslides and many scholars have studied the classification of landslides over the years. Classification of landslides according to material composition is one of the most commonly used means of classification at home and abroad, classifying landslides into rocky and soil landslides, of which soil landslides include stockpiled soil landslides, loess landslides, clayey soil landslides, and landfill landslides, etc. Varnes (1978) [20] categorized slope movements based on rock and soil movement characteristics into falls, topples, slides, lateral spreads, flows, and complex movements. Liu Guangrun (1992) [21], in his study on major geological and seismic issues in the Three Gorges of the Yangtze River, classified slope structures based on the relationship between structural planes and the slope surface into dip-slope normal, dip-slope reverse, and inverse slope types. Liu Guangrun and Xu Kaixiang (1993) divided slope deformations into natural and anthropogenic dynamics based on different causative factors. Wang Lansheng, Zhang Zhuoyuan, et al. (1994) [22] proposed five basic combination models for the deformation mechanism of slopes composed of layered or layer-containing rock bodies: creep-shear, slip-induced tension cracking, bending-tension cracking, plastic flow-tension cracking, and slip-bending. Yan Tongzhen et al. (1994, 2000) [23] summarized nine types of sliding mechanisms based on the initial conditions, fundamental causes, and apparent sliding modes of landslides: rheological overturning landslide, stress release translational landslide, vibration collapse or liquefaction landslide, subsidence landslide due to erosion, geochemical suspension-sinking landslide, high potential energy leapfrog landslide, pore water pressure floatation landslide, erosion-loading landslide, and giant high-speed long-runout landslide. Liu Guangrun et al. (2002) [24,25] proposed a comprehensive and systematic landslide classification system for the first time, based on the characteristics of the landslide body, deformation dynamics, and activity features, offering a detailed classification of landslides.

In recent years, the landslide classification system has continually evolved and developed, gradually forming a comprehensive classification system based on “category, size, type, mode, and stage”. The type of landslide mass (material structural composition) is classified by “category”, which includes rock landslides, soil landslides, and accumulation layer landslides, further subdivided based on material composition and the relationship between structural planes and slope surfaces. Rock landslides include rock layer-conformable, rock layer-nonconformable, and rock cross-layer landslides. Soil landslides include loess, clayey soil, and man-made fill landslides. Accumulation layer landslides include colluvium and talus landslides. The scale of the landslide is categorized by “size”, dividing landslides into nine types based on landslide volume and landslide mass thickness, ranging from small to gigantic, and shallow to super-deep. The causative forces are classified by “type”, with nine types of causative forces divided into natural and anthropogenic. The deformation movement characteristics and failure modes are sorted by “mode”, classifying landslides based on kinematic features, dynamic characteristics, and deformation failure modes. The development stage of the landslide is classified by “stage”, distinguishing between new and reactivated landslides in terms of their evolutionary stages. The research group based on the aforementioned geological model carries out a refined classification of accumulation layer landslides in the middle Qinling–Bashan Mountains (Figure 1).

2.2. Model Construction Method

For on-site landslide monitoring data, processing such as data partitioning is performed. According to the characteristics of time variables, data can be divided into time-series and non-time-series data, and preprocessing is conducted based on the unique attributes of the two datasets. The landslide basic survey table records non-time-series data, including landslide scale, thickness, volume, quantity, and basic information on deformation movement characteristics. On the other hand, landslide monitoring data, such as surface displacement, rainfall, and tilt, constitute time-series data. The model needs to be capable of processing time-series data while also possessing good interpretability to assist professional technical personnel in monitoring and early warning of geological

disasters, and understanding the influencing factors in landslide deformation [26]. Deep learning models have difficulty interpreting the relationship between prediction results and input features.

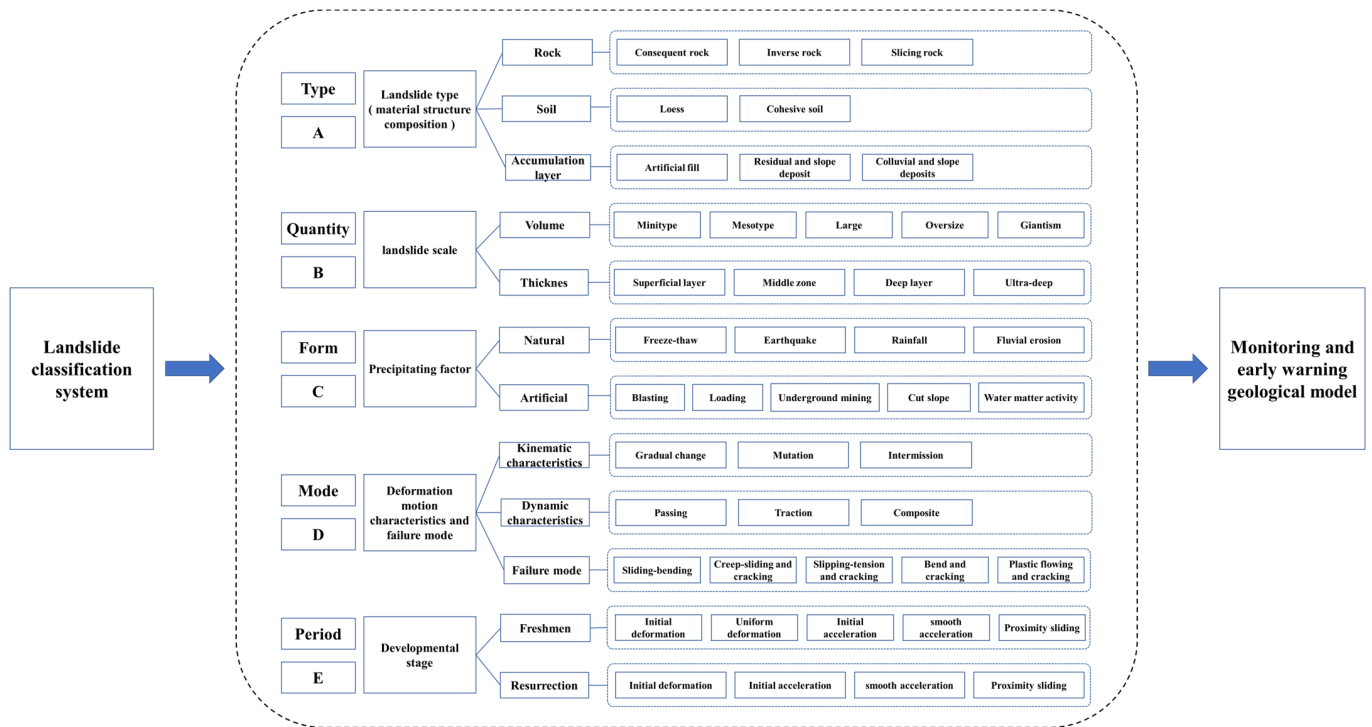


Figure 1. Geological model for classifying landslides in the middle Qinling–Bashan Mountains area with stacked layers.

Predictive methods based on individual slopes are closely related to historical data and struggle to reveal the characteristics of landslide movement over the complete lifecycle. Similar-type landslide prediction models consider the interpretability of the model, the landslide’s primary influencing factors, and the characteristics of landslide movement throughout the lifecycle of similar landslides to construct a predictive model based on the concept of similar-type landslides. This predictive model mainly consists of two steps: the first step uses the XGBoost machine learning model for feature importance analysis, with the analyzed results serving as feature input for subsequent deformation prediction. The second step employs the LSTM deep learning model to output predictions.

The XGBoost decision tree algorithm [27] can calculate the importance of each input feature to the final prediction result. The greater the weight of feature importance, the more significant its impact on the prediction outcome. Thus, this model is selected for feature importance analysis. Additionally, XGBoost is known for its efficiency, flexibility, and robustness: it employs parallel processing to rapidly train large datasets, it can handle both numerical and categorical features, and it is capable of managing missing values.

The XGBoost objective function is shown in Equation (1):

$$L(\phi) = \sum_i l(y_i, \hat{y}_i) + \sum_k \Omega(f_k) \tag{1}$$

where $\Omega(f_k)$ as shown in Equation (2):

$$\Omega(f_k) = \gamma T + \frac{1}{2} \lambda \|\omega\|^2 \tag{2}$$

contains the regularization term, \hat{y}_i is the output of the model, y_i is the true label, f_k denotes the k th base classifier, T is the number of leaves in the tree, ω denotes the score in the corresponding leaves, and γ is the penalty term.

Expanding Equation (1) using Taylor’s formula yields Equation (3):

$$L^{(t)} = \sum_{i=1}^n \left[g_i f_t(x_i) + \frac{1}{2} h_t f_t^2(x_i) \right] + \Omega(f_t) \tag{3}$$

The formula g_i is the same as h_t and $\Omega(f_t)$. The expression equations are Equations (4)–(6), respectively, as follows:

$$g_i = \partial_{\hat{y}_i^{(t-1)}} l(y_i, \hat{y}_i^{(t-1)}) \tag{4}$$

$$h_i = \partial_{\hat{y}_i^{(t-1)}}^2 l(y_i, \hat{y}_i^{(t-1)}) \tag{5}$$

$$\Omega(f_t) = \gamma T + \frac{1}{2} \lambda \sum_{j=1}^T \omega_j^2 \tag{6}$$

Substituting Equations (4)–(6) into Equation (3) yields the leaf node weight formula shown in Equation (7):

$$\omega_j^* = -\frac{G_j}{H_j + \lambda} \tag{7}$$

G_j and H_j denote the values of first-order gradient and second-order gradient at the leaf nodes, respectively; the optimal solution of the objective function is obtained by bringing Equation (7) into Equation (3) as shown in Equation (8):

$$\hat{L}^* = -\frac{1}{2} \sum_{j=1}^T \frac{G_j^2}{H_j + \lambda} + \gamma T \tag{8}$$

Landslide deformation prediction primarily focuses on forecasting time-series data for surface displacement [28]. The Long Short-Term Memory (LSTM) network algorithm, compared to traditional Recurrent Neural Networks (RNNs), is more adept at addressing gradient vanishing problems in long sequences. It can handle longer sequence data and better capture long-term dependencies within sequential data. Its time sensitivity enables more effective learning of the features in time-series data [29]. The plan is to apply a hybrid XGBoost and LSTM model to landslide deformation prediction to enhance the accuracy of predictions while also achieving model interpretability [30–32].

LSTM [33] introduces a memory cell that stores and accesses information and controls the flow of information through a gating mechanism. The key parts of LSTM include input gate, forget gate, and output gate (Figure 2).

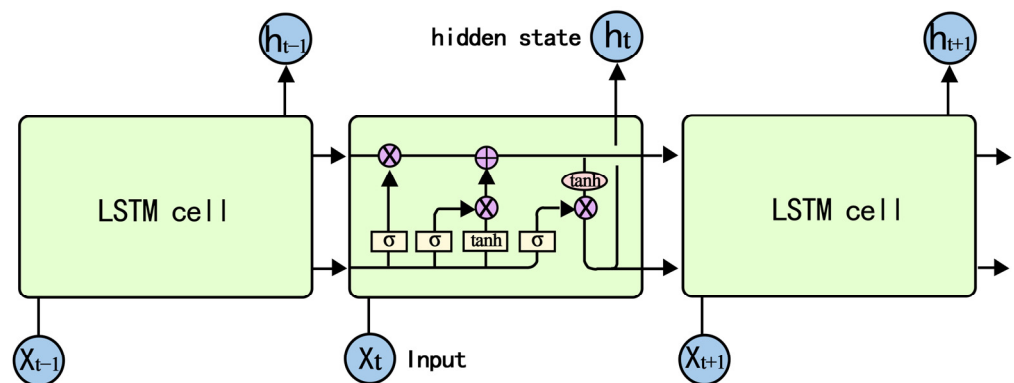


Figure 2. LSTM model.

- Forget gate

The first step in LSTM is to decide what information we need to throw away from the cell state. This decision is made by a sigmoid layer called the forget gate. With the inputs h_{t-1} and x_t it outputs a number between 0 and 1. An output of 1 means “keep this value completely” and 0 means “throw this value away completely”.

The forgetting gate is calculated as in Equation (9).

$$f_t = \sigma(W_f \cdot [h_{t-1}, x_t]) + b_f \quad (9)$$

- Input gate

The second step is to decide what kind of information we need to store in the cell state. There are two parts to this problem. First, the sigmoid layer calls an “input gate” to decide what data needs to be updated. Then, a $\tan h$ layer creates a vector \tilde{C}_t as new candidate value that can be added to the state. In the next step, we want to merge these two parts to create an update to the state.

The input gate is calculated as in Equations (10) and (11):

$$i_t = \sigma(W_i \cdot [h_{t-1}, x_t]) + b_i \quad (10)$$

$$\tilde{C}_t = \tan h(W_c \cdot [h_{t-1}, x_t]) + b_c \quad (11)$$

The forgetting gate and input gate are combined as in Equation (12):

$$C_t = f_t * C_{t-1} + i_t * \tilde{C}_t \quad (12)$$

- Output gate

Finally, we need to decide what we want to output. This output is based on our cell state but will be a filtered value.

The output gate is calculated as in Equations (13) and (14):

$$o_t = \sigma(W_o \cdot [h_{t-1}, x_t]) + b_o \quad (13)$$

$$h_t = o_t * \tan h(C_t) \quad (14)$$

2.3. Selection of Evaluation Indicators

In order to analyze and study the prediction ability of the displacement monitoring data model, the model test uses two assessment indicators, MSE and MAPE, to measure the model prediction effect.

MSE squares the difference between the predicted and actual values for each time period, and then averages the squares of the differences over multiple time periods to obtain the average mean square error. The MSE metric has the advantage of being able to highlight extreme errors, as in Equation (15).

$$MSE = \frac{1}{n} \sum_{i=1}^n (Y_i - \hat{Y}_i)^2 \quad (15)$$

MAPE denotes the mean percentage of direct relative error between predicted and measured values in the range $[0, +\infty)$; the smaller it is the more accurate the prediction model is, as in Equation (16).

$$MAPE = \frac{100\%}{n} \sum_{i=1}^n \left| \frac{\hat{y}_i - y_i}{y_i} \right| \quad (16)$$

3. Research Case

The middle Qinling–Bashan Mountains is located in the Qinling Mountains and Bashan Mountain Range in southern Shaanxi, ranges from $31^{\circ}42' N$ to $34^{\circ}33' N$ and from $105^{\circ}29' E$ to $111^{\circ}15' E$ (Figure 3), and is mainly located in the cities of Hanzhong, Ankang, and Shangluo in southern Shaanxi (Figure 3). The average annual temperature in the study area is $11\text{--}14^{\circ}C$ and the annual precipitation is $750\text{--}1000\text{ mm}$, which is mostly concentrated in July–September each year, accounting for about 50% of the annual precipitation, during which torrential rains and continuous rainy weather are predominant.

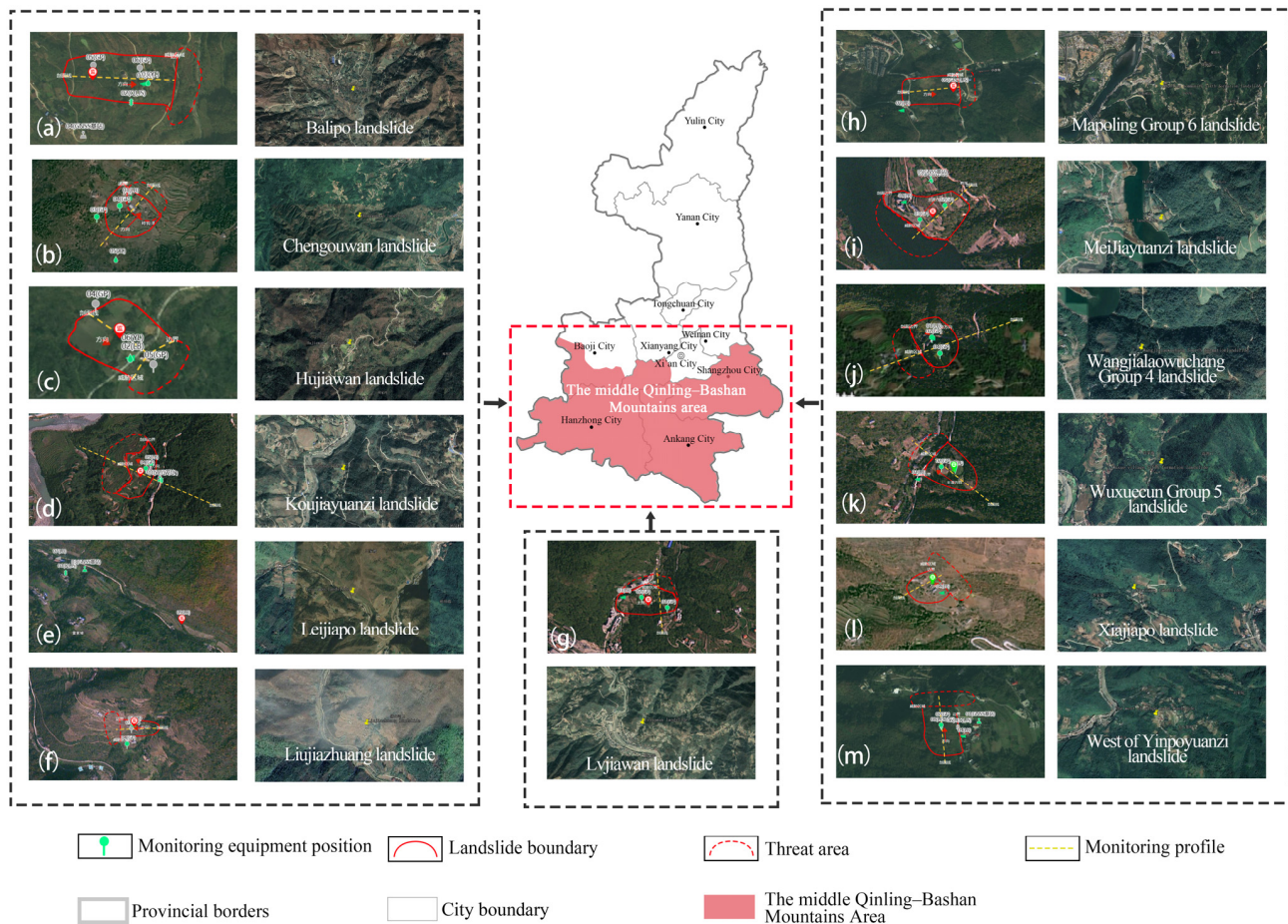


Figure 3. Location of the middle Qinling–Bashan Mountains Area and basic information on landslide monitoring. (a) Balipo landslide. (b) Chengouwan landslide. (c) Huijiawan landslide. (d) Koujiayuanzi landslide. (e) Leijiapo landslide. (f) Liujiazhuang landslide. (g) Lvjiawan landslide. (h) Mapoling Group 6 landslide. (i) MeiJiayuanzi landslide. (j) Wangjialaowuchang Group 4 landslide. (k) Wuxuecun Group 5 landslide. (l) Xiajiapo landslide. (m) West of Yinpoyuanzi landslide.

The geomorphology of the Qinling–Bashan Mountains area belongs to low, middle, and high mountains and wide valley basin landforms, with altitudes ranging from 170 to 3000 m above sea level, and a series of subsidence basins have been formed by the fracture and subsidence action of the landmass. The middle Qinling–Bashan Mountains area is a multiplate convergence zone; the plates squeeze each other, the ground stress is extremely complex, the rock deformation is strong, faults and folds are extremely developed, and the peak acceleration of the ground vibration is generally 0.05 g . The region is subject to intense tectonic movement, resulting in the stacking and interweaving of tectonic plates, which leads to an extremely complex distribution of rock types. The predominant lithologies in the area are Quaternary unconsolidated deposits, slate, and phyllite. Groundwater in the area primarily forms through the vertical infiltration of atmospheric precipitation.

Its movement and storage vary with depth, with shallow layers typically containing unconsolidated sediment pore water and deeper layers hosting bedrock fracture water. Human engineering activities in the area are mainly focused on housing construction, road building, and mining. The region is characterized by high mountains, deep valleys, and steep slopes, and is rife with geological structures such as faults. Additionally, concentrated rainfall and high cumulative precipitation volumes make this region highly susceptible to geological hazards. Rock types such as slate, schist, and phyllite, which are prone to slipping, as well as Quaternary slope debris accumulations and expansive soils, are widely distributed. Investigation and analysis show that geological hazards in the region exhibit interannual and monthly patterns, with more incidents occurring in wet years and fewer during dry years. The vast majority of landslides, collapses, and unstable slope failures are concentrated in the rainy season, with statistical data indicating that about 80% occur between July and September [34–37].

By the end of 2022, the region had a total of 6084 registered geologic hazard sites, posing a potential threat to the safety of 165,636 people and about CNY 1.4 billion worth of property. Among these hazards, landslides accounted for the highest proportion at 89.6%, followed by collapses at 4.9%, debris flows at 4.7%, and other types at 0.7%.

Landslides in the middle Qinling–Bashan Mountains are predominantly medium- and small-scale accumulation layer landslides. The material of these landslide masses mainly consists of clay, silt, silty clay, and gravel of various sizes. The sliding surfaces are generally at the contact between bedrock and accumulation layer material, or along interfaces of bedrock with different degrees of weathering. The landslides are significantly influenced by heavy summer rainfall and human engineering activities. The main disaster evolution pattern of landslides in this central section is creep–shear, with the primary evolutionary process detailed in Table 1. These types of accumulation layer landslides have a relatively long deformation evolution process, allowing for the collection of long-term time-series displacement monitoring data, making them suitable for machine learning applications.

Table 1. Creep–slip–pull-type evolutionary model of landslides in the middle portion of the accumulation layer in the Qinling–Bashan Mountains area.

State of Affairs	Schematic Diagram of the Evolution of the Pattern of Disasters	Characterization
Natural state		The original slope is in its natural state, with the surface of the slope exposed, and the strongly weathered and moderately weathered surfaces of the slope are potential sliding surfaces.
Accelerated weathering		Accelerated weathering of slopes from surface to depth
Stress concentration		Concentration of stresses at the foot of slopes and gradual decrease in stability
Landslide formation		Sliding surface penetrates, slide falls, landslide forms.

The research objects for this study in the middle Qinling–Bashan Mountains are accumulation layer landslides selected from automated geological hazard monitoring sites within the region. After analyzing and comparing data, 13 landslides equipped with rain gauges and surface displacement devices, and showing clear deformation trends were chosen to construct the dataset. These include the Balipo landslide, Chengouwan landslide, Hujiawan landslide, Koujiayuanzi landslide, Leijiapo landslide, Liujiazhuang landslide, Lvjiawan landslide, Mapoling Group 6 landslide, MeiJiayuanzi landslide, Wangjialaowuchang Group 4 landslide, Wuxuecun Group 5 landslide, Xiajiapo landslide, and West of Yin-poyuanzi landslide (Figures 4–7). The 13 landslides were classified according to the geological model established in Figure 1 (Table 2) and can be subdivided into seven types: new traction type colluvial landslide, new traction type talus landslide, new translational type colluvial landslide, reactivated translational type talus landslide, reactivated translational type broken accumulation landslide, reactivated traction type colluvial landslide, and reactivated traction type talus landslide. The classification codes are as shown in Table 3.

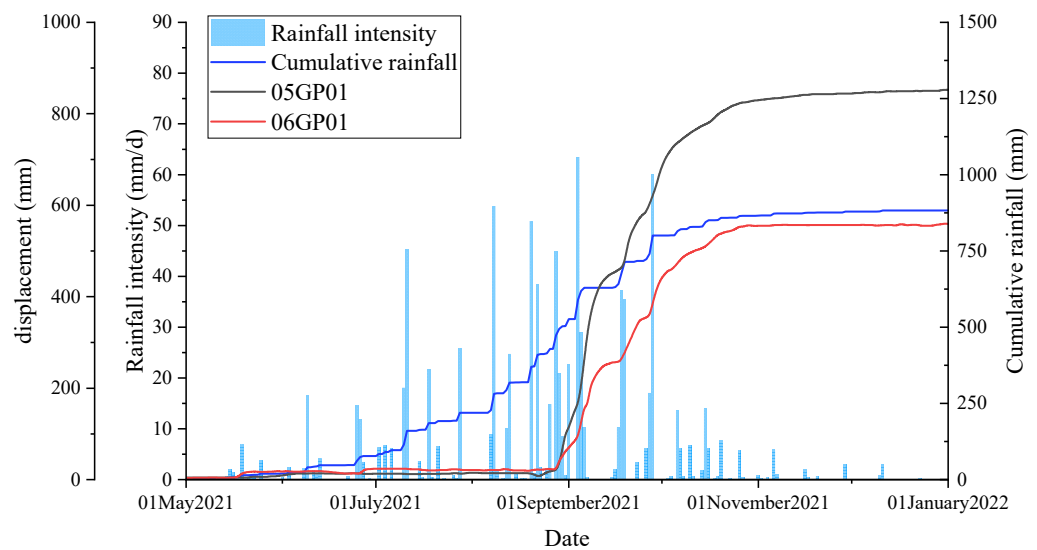


Figure 4. Rainfall-displacement monitoring data of Balipo landslide.

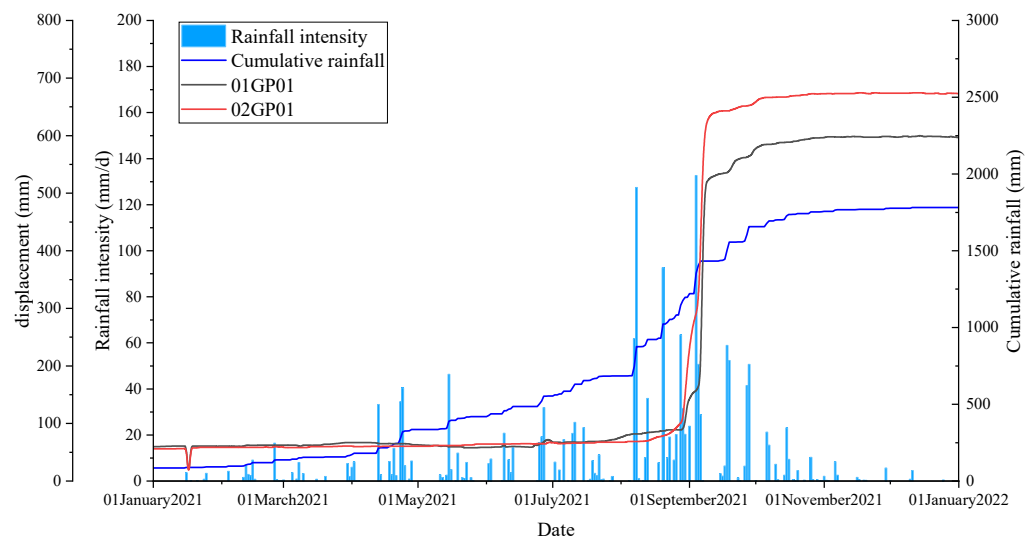


Figure 5. Rainfall-displacement monitoring data of Lvjiawan landslide.

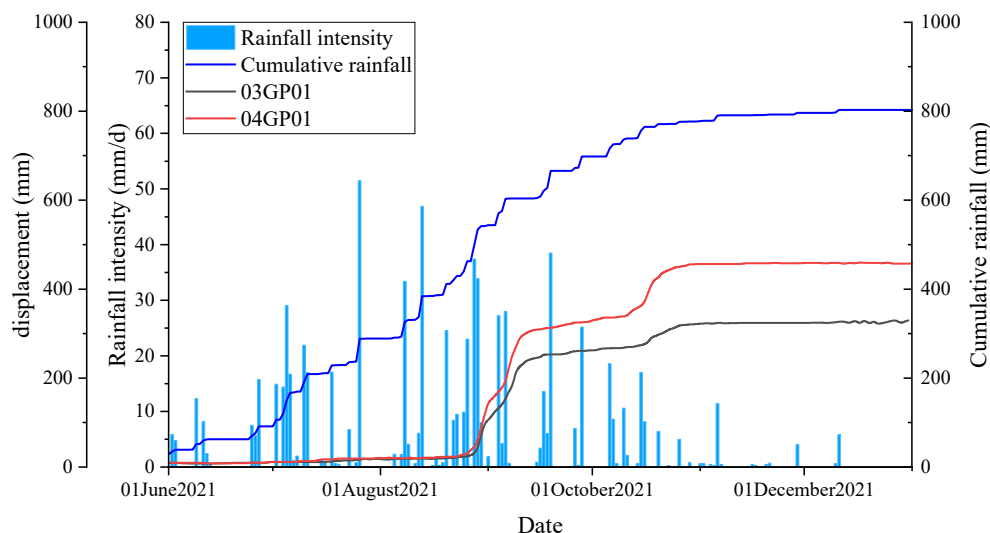


Figure 6. Rainfall-displacement monitoring data for the Chengouwan landslide.

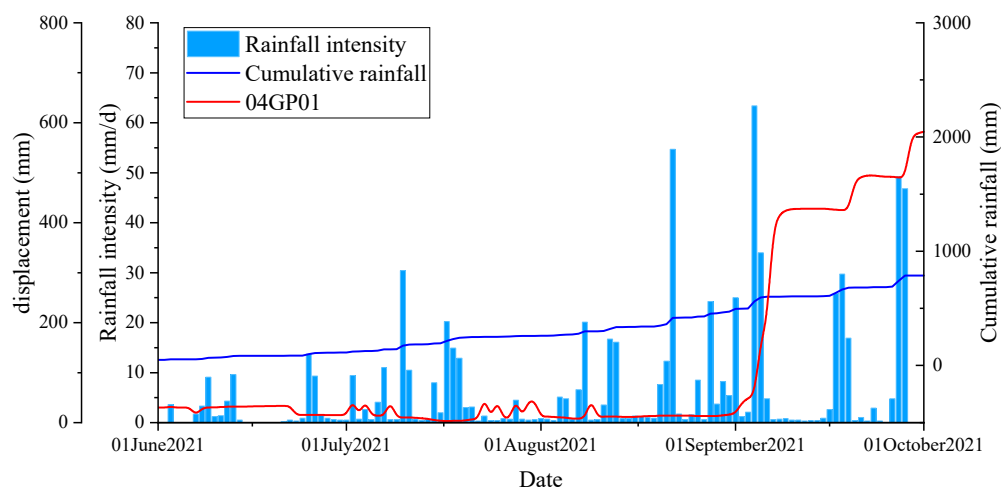


Figure 7. Rainfall-displacement monitoring data of Leijiapo landslide.

Table 2. Refined classification of landslides in the middle Qinling–Bashan Mountains region of the accumulation layer.

Name of the Landslide	Structural Composition of Matter	Landslide Size (Large, Medium, Small)	Predisposing Factors (Kinetic Causes)	Kinematic Characteristics (Gradual, Abrupt, Intermittent)	Kinetic Characterization (Traction, Nudge, Composite)	Developmental Stages (New, Resurrection)
Balipo landslide	Remnant slope product	Medium-sized	Rainfall	Abrupt	Traction	New
Chengouwan landslide	Landslide	Minor works	Rainfall	Abrupt	Traction	New
Hujiawan landslide	Slope failure	Minor works	Rainfall	Abrupt	Nudge	Resurrection
Koujiayuanzi landslide	Remnant slope product	Medium-sized	Rainfall	Abrupt	Traction	Resurrection
Lei Jiapo landslide	Slope failure	Minor works	Rainfall	Abrupt	Traction	Resurrection
Liujiazhuang landslide	Remnant slope product	Minor works	Rainfall	Abrupt	Nudge	New

Table 2. Cont.

Name of the Landslide	Structural Composition of Matter	Landslide Size (Large, Medium, Small)	Predisposing Factors (Kinetic Causes)	Kinematic Characteristics (Gradual, Abrupt, Intermittent)	Kinetic Characterization (Traction, Nudge, Composite)	Developmental Stages (New, Resurrection)
Lvjiawan landslide	Landslide	Medium-sized	Rainfall	Abrupt	Nudge	Resurrection
Mapoling Group 6 landslide	Remnant slope product	Medium-sized	Rainfall	Abrupt	Traction	New
Meijiayuanzi landslide	Landslide	Medium-sized	Rainfall	Abrupt	Traction	Resurrection
Wangjialao-wuchang Group 4 landslide	Landslide	Medium-sized	Rainfall	Abrupt	Nudge	Resurrection
Wuxuecun Group 5 landslide	Landslide	Minor works	Rainfall	Abrupt	Traction	Resurrection
Xiajiapo landslide	Landslide	Minor works	Rainfall	Abrupt	Traction	Resurrection
West of Yinpo Yuanzi landslide	Landslide	Minor works	Rainfall	Abrupt	Traction	Resurrection

Table 3. Refined classification codes for landslides in the middle Qinling–Bashan mountains area.

Classification Code	Type of Landslide	Name of the Landslide
1	Emerging traction residual landslides	Balipo landslide, Mapoling Group 6 landslide
2	Emerging traction avalanche landslides	Chengouwan landslide
3	Emergent nudge-type residual landslides	Liujiashuang landslide
4	Resurrection of a nudging avalanche-accumulated landslide	Hujiawan landslide, Wangjialaowuchang Group 4 landslide
5	Resurrection of a nudging debris slide	Lvjiawan landslide
6	Resurrection of traction residual landslides	Koujiayuanzi landslide
7	Resurrection of a traction avalanche landslide	Leijapo landslide, Meijiayuanzi landslide, Wuxuecun Group 5 landslide, Xiajiapo landslide, West of Yinpo Yuanzi landslide

4. Comparative Experiments on Group Prediction

4.1. Experimental Process

The research team conducted machine learning experiments based on the 13 landslide accumulation layers selected from in the middle Qinling-Bashan mountains area mentioned earlier, carrying out comparative analysis work on deformation prediction for similar-type landslides and mixed-type landslides. In the first group of experiments (Table 4), the training dataset for similar-type landslides consisted entirely of Type 7 landslides, which also represented the most numerous type in this dataset. The training dataset for mixed-type landslides included landslides of types other than 7. In the second group of experiments (Table 5), the training dataset for similar-type landslides was entirely composed of Type 7 (including historical monitoring data of West of Yinpo Yuanzi landslide), while the training dataset for individual slope landslides was based on historical monitoring data of the landslide on the west of the Yinpo yard. The prediction set for all experiments used the data from West of Yinpo Yuanzi landslide.

Table 4. First group of experiments.

Experiments	Prediction of Similar Landslides		Mixed Category Landslide Prediction	
	Name of the Landslide	Classification Code	Name of the Landslide	Classification Code
Training set	Leijiapo landslide	7	Ba Lipo landslide	1
	Meijiayuanzi landslide	7	Chengouwan landslide	2
	Wuxuecun Group 5 landslide	7	Liujiazhuang landslide	3
	Xiajiapo landslide	7	Hujiawan landslide	4
Prediction set	West of Yinpoyuanzi landslide	7	West of Yinpoyuanzi landslide	7

Table 5. Second group of experiments.

Experiments	Prediction of Similar Landslides		Single-Slope Landslide Prediction	
	Name of the Landslide	Classification Code	Name of the Landslide	Classification Code
Training set	Leijiapo landslide	7	West of Yinpoyuanzi landslide	7
	Meijiayuanzi landslide	7		
	Wuxuecun Group 5 landslide	7		
	Xiajiapo landslide	7		
	West of Yinpoyuanzi landslide	7		
Prediction set	West of Yinpoyuanzi landslide	7	West of Yinpoyuanzi landslide	7

4.2. Key Feature Selection

Due to the abnormal power supply of equipment in the field, the failure of the equipment itself, or the weak communication signal causing the monitoring data to jump or be missing, the first step is to carry out the cleaning of landslide deformation monitoring data, including the filling of missing data and correction of abnormal data [38–42]. Due to the diversity of geohazard monitoring data, it is difficult to completely identify abnormal data with the same algorithm [43,44]. In order to identify the anomalous data, the long time series of monitoring data is processed using the method of region segmentation and the specific algorithm for different morphology data is used to identify the anomalies. For data with smooth morphology, the 3σ criterion and isolated forest are used to eliminate the anomalous data. For data segments characterized by a clear trend, a least squares polynomial curve is used to fit the trend line.

Landslide deformation is a complex multidimensional nonlinear movement, which is the result of a variety of factors, and it is necessary to deeply explore the features of landslide deformation and the triggering factors affecting the deformation, such as rainfall on the same day, effective rainfall, slope, volume type, thickness type, structural type, deformation movement characteristics, and development stage. Due to the large amount of feature data, if all of them are used as input items of the model, the problem of dimensional catastrophe will occur, which will weaken the accuracy and generalization ability of the model, and lead to a decrease in the accuracy of the model. Our research group selects the random forest XGBoost machine learning algorithm in the embedding method to screen all the features (Table 6) and screens out the features in the feature data that have higher correlation with the stage of landslide displacement change, so as to get the subset of features for the input of the prediction and early warning model, which reduces the dimensionality of the input features of the landslide prediction and early warning model, and improves the model precision and generalizability.

The machine learning results are as follows: rainfall contributes about 55%, volume contributes about 13%, thickness contributes about 12%, slope contributes about 11%, material structure contributes about 9%, and other features are negligible. From there, the above features were selected as influencing factors for the inputs to the late deformation prediction model (Figures 8 and 9).

Table 6. Selected feature terms.

Data Item Name	Data Type	Note
Timing	Timestamp	Sampling frequency in hours
R	Continuous data	Rainfall for the day
R1	Continuous data	Rainfall for the previous 1 day
R2	Continuous data	Rainfall for the first 2 days
R3	Continuous data	Rainfall for the first 3 days
Volume	String class data	Small, medium, large
Thicknesses	String class data	Shallow, medium, deep
Structural of matter	String class data	Slope failure, slope remnants
Elevation	String class data	Class I (slope $\leq 15^\circ$), Class II ($15^\circ \leq \text{slope} \leq 30^\circ$), Class III ($35^\circ \leq \text{slope} \leq 60^\circ$), Class IV (slope $\geq 60^\circ$)
Kinetic characteristics	String class data	Towed, pushed
Developmental stage	String class data	New, resurrection
Fissures	Discrete ordered data	No, yes

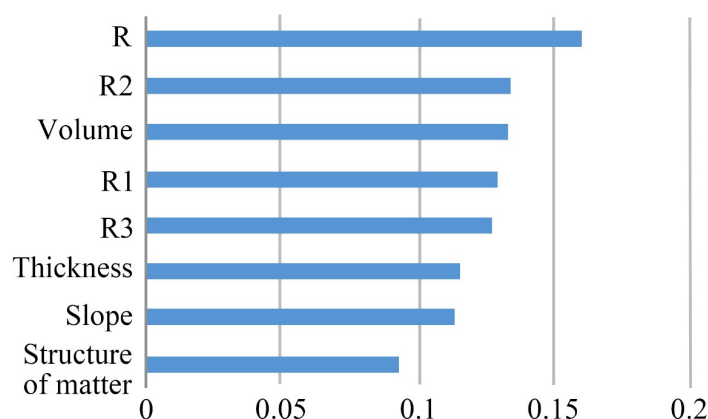


Figure 8. Characteristic importance assessment.

4.3. Analysis of Results and Discussion

In order to keep the experiments comparable, the structure, hyperparameters, and amount of training data are the same for the three sets of models, which predict landslide displacements after 12 h, 24 h, and 48 h, respectively. The number of past data referenced for prediction is 18 (6 h unit), learning rate is 0.0002, and number of epochs is 300. The size of hidden size of the LSTM model is 512 and the number of training data in a single batch is 24. The optimal hyperparameters of the model are selected by using the grid search method in the experiments. The evaluation indexes of the two sets of experimental results are shown in the table, and some of the prediction effects are shown in Tables 7 and 8 and Figures 10–12.

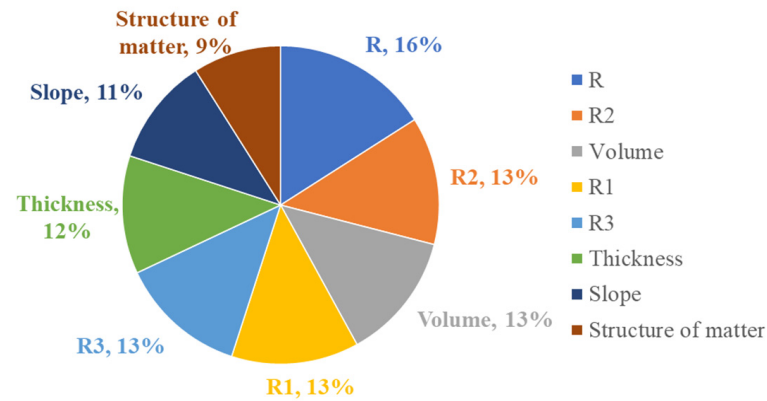


Figure 9. Characteristic contribution percentage.

The first experiment’s similar-type landslide prediction model showed optimal performance in predicting the next 12 h on the test set, with an MSE of 5.036 and a MAPE of 0.01. Under the same training conditions and predicting the same duration, the joint training of similar-type landslides yielded better results than the joint training of mixed-type landslides.

In the second experiment, the similar-type landslide prediction model exhibited the best performance in predicting the next 12 h on the test set, with an MSE of 5.099 and a MAPE of 0.01. However, for predicting the next 24 and 48 h, the individual slope landslide prediction model outperformed the similar-type landslide prediction model.

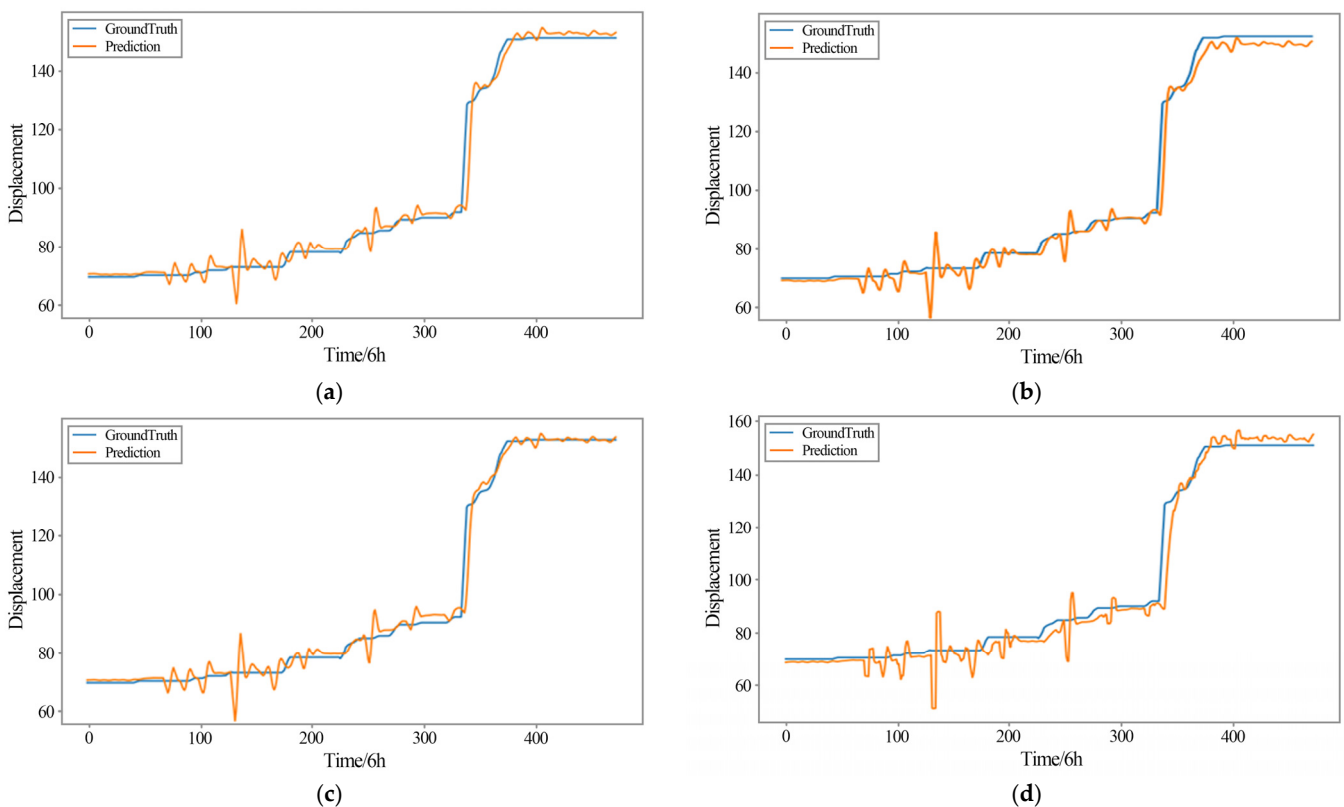


Figure 10. Subgroups predicting effects over the next 12 h. (a) First set of similar slopes projected for the next 12 h. (b) First set of mixed slopes projected for the next 12 h. (c) Second set of similar slopes projections for the next 12 h. (d) Second set of single-slope projected for the next 12 h.

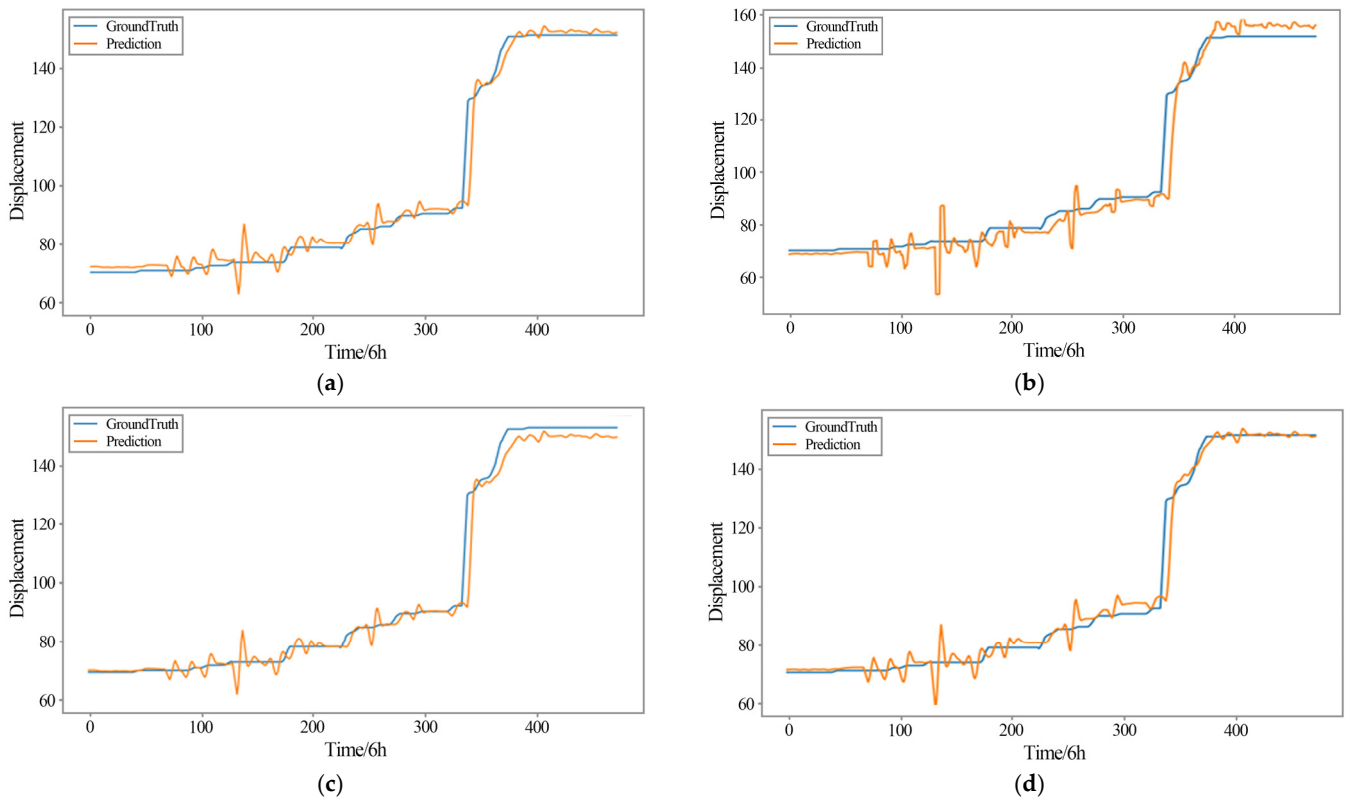


Figure 11. Subgroups predicting effects over the next 24 h. (a) First set of similar slopes projected for the next 24 h. (b) First set of mixed slopes projected for the next 24 h. (c) Second set of similar slopes projections for the next 24 h. (d) Second set of single-slope projected for the next 24 h.

A comparison of the two sets of experiments reveals that (1) under the same amount of training data, in most cases, the shorter the prediction duration of the same model, the higher the accuracy; (2) for a 12 h prediction, the similar-type landslide prediction model performs best, followed by the individual slope landslide model, and then the mixed-type landslide model; (3) for 24 h and 48 h predictions, the individual slope landslide prediction model performs best, followed by the similar-type landslide model and then the mixed-type landslide model; (4) both the similar-type landslide prediction model and the individual slope landslide prediction model perform relatively well. Especially in terms of the MAPE metric, the prediction accuracy of the similar-type landslide model is consistent with that of the individual slope landslide model.

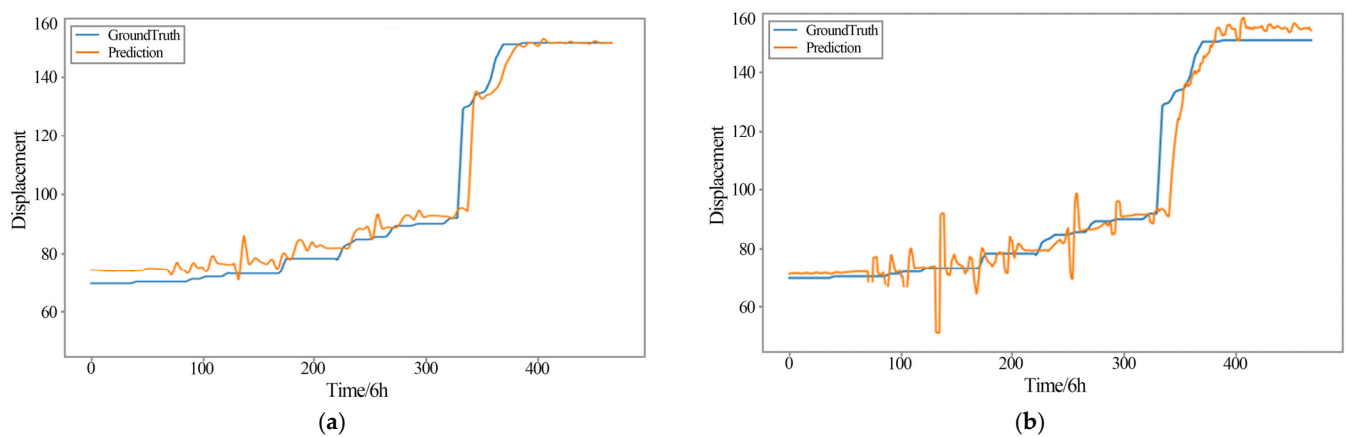


Figure 12. Cont.

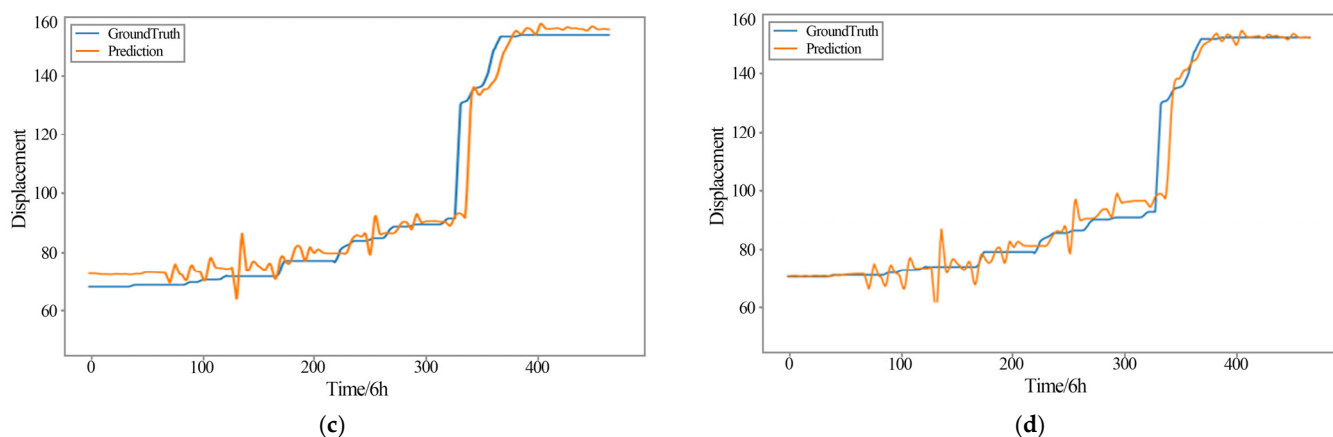


Figure 12. Subgroups predicting effects over the next 48 h. (a) First set of similar slopes projected for the next 48 h. (b) First set of mixed slopes projected for the next 48 h. (c) Second set of similar slopes projections for the next 48 h. (d) Second set of single-slope projected for the next 48 h.

Analyzing the different results for predicting 12 h versus 24 and 48 h in the second group, the reason may be that the individual slope landslide has already gone through three stages: initial deformation, uniform deformation, and accelerated deformation. With a sufficient amount of training sample data, the individual slope landslide prediction model has learned the characteristics of different evolutionary stages, hence the better prediction performance, not fully demonstrating the advantage of joint training of similar-type landslides.

Table 7. Evaluation indicators of the results of the first group of experiments.

Group I Homogeneous Slopes	MSE	MAPE	A Set of Mixed Slopes	MSE	MAPE
Next 12 h	5.036	0.010	Next 12 h	7.616	0.024
Next 24 h	7.333	0.0142	The next 24 h	11.085	0.027
Next 48 h	15.232	0.022	The next 48 h	20.670	0.033

Table 8. Evaluation indicators of the results of the second group of experiments.

Group II Homogeneous Slopes	MSE	MAPE	Group II Single Slope	MSE	MAPE
Next 12 h	5.099	0.010	Next 12 h	6.069	0.017
Next 24 h	7.242	0.0141	Next 24 h	6.397	0.018
Next 48 h	14.928	0.0212	Next 48 h	6.110	0.018

5. Discussion

This paper presents a study on the displacement prediction of similar-type landslides in the middle Qinling–Bashan Mountains, focusing on accumulation layer landslides. The enhancement of prediction accuracy necessitates the use of prolonged and continuous monitoring data for model refinement. The methods employed for landslide classification, model construction, and prediction provide a reference for displacement prediction of landslides in other regions and of different types. The use of similar-type landslide prediction models to supplement data enables the acquisition of sliding characteristics at different evolutionary stages of landslides, offering a scientific basis for early landslide prediction and warning.

The study proposes a machine-learning-based method for constructing similar-type landslide deformation prediction models, based on the premise that similar landslides exhibit analogous movement characteristics. This approach includes key steps such as

landslide classification methods, feature importance analysis and selection, construction of training sample sets, and sample learning training with optimization and model tuning. A monitoring and early warning geological model based on landslide classification is proposed, encompassing the structure, scale, inducing factors, deformation movement characteristics, failure modes, and development cycles of the landslide body. This refined classification provides a basis of expert knowledge and experience for machine learning. Furthermore, the study introduces a method combining XGBoost and LSTM models for landslide deformation prediction, enhancing the accuracy of the predictions while achieving model interpretability. The XGBoost model is used to analyze the main features of landslide deformation, which are then incorporated as input features in the training of the samples. The contribution of rainfall is approximately 55%, volume around 13%, thickness 12%, slope gradient about 11%, and material structure around 9%, with other features being negligible.

The refined classification of landslides requires manual intervention and is closely related to the experience of the researchers, leading to variability in results among different researchers, which can influence the final landslide displacement predictions. The predictive results for different landslides are closely related to the developmental stage of the landslides and are significantly correlated with the developmental stage and quality of monitoring data of similar landslides in the study area. Regions with high landslide susceptibility and widespread displacement monitoring tend to have better predictive outcomes, suggesting the potential for adoption and wider application of these methods. The predictive method proposed in this paper requires a substantial amount of long-term continuous observational data as samples for machine learning. The requirements for deformation prediction are relatively high and the applicability of these methods is somewhat limited. The predictive results are highly correlated with the duration and quality of the monitoring data, and the predictive models require continuous refinement to be truly effective.

6. Conclusions

This paper presents a method and process for constructing a prediction model for deformation in similar-type landslides. Taking the landslide accumulation layers in the middle Qinling–Bashan Mountains area as an example, a training sample set for these landslides was constructed. A data-driven deformation prediction model for the middle section of the Qinling–Bashan Mountains area's accumulation layers was developed, utilizing historical monitoring data and key feature parameters of similar-type landslides for predicting future 12 h, 24 h, and 48 h deformations. The model's predictive performance was also evaluated. The main conclusions of this study are as follows:

1. The displacement prediction model for similar-type landslides performs better in displacement prediction than the mixed-type landslide prediction model.
2. The displacement prediction models for similar-type landslides and individual slope landslides tend to converge in performance. For predicting displacement in the next 12 h, the similar-type landslide model outperforms the individual slope model. The effectiveness of longer-duration predictions is closely related to the developmental stage of the predicted landslide.
3. The similar-type landslide displacement prediction model can learn the sliding characteristics of landslides at different evolutionary stages, providing a scientific basis for early prediction and warning of landslides. It effectively addresses the issues of insufficient early monitoring data and low prediction accuracy in landslide monitoring.

Author Contributions: Conceptualization, J.M., Q.Y. and M.Z.; Methodology, J.M., Q.Y. and M.Z.; Software, C.O.; Validation, Q.Y. and M.Z.; Formal analysis, Q.Y. and M.Z.; Investigation, J.M., Q.Y., M.Z. and D.M.; Resources, J.M., Q.Y. and M.Z.; Data curation, J.M., Q.Y., M.Z. and W.Z.; Writing—original draft, J.M., Q.Y. and M.Z.; Writing—review & editing, J.M., Q.Y., M.Z. and Y.C.; Visualization, Q.Y.; Supervision, J.M., Q.Y. and M.Z.; Project administration, J.M., Q.Y. and M.Z.; Funding acquisition, M.Z. All authors have read and agreed to the published version of the manuscript.

Funding: This study was financially supported by the National Natural Science Foundation of China (No. 42371379), the National Key Research and Development Program (No. 2022YFB3903604), Fundamental Research Funds for the Central Universities (No. 2652023001), the Geological Survey Program of China (No. DD20211364).

Data Availability Statement: The data presented in this study are all available in the article.

Acknowledgments: The authors are thankful to the reviewers for their constructive suggestions on improving the manuscript.

Conflicts of Interest: Prof. Dr. Qiang Yang was employed by the China Institute of Geo-Environment Monitoring Co., Ltd and Mr. Chengyu Ouyang was employed by Wuhan Infoearth Information Engineering Co., Ltd. The remaining authors declare that the research was conducted in the absence of any commercial or financial relationships that could be construed as a potential conflict of interest.

References

1. Fan, L.M.; He, J.J.; Li, C.G. Study on development patterns of landslide in Qinling-Bashan Mountains. *Chin. J. Geol. Hazard Control* **2004**, *15*, 47–51.
2. Sun, G.M.; Kuang, M.S.; Qu, H. Research of Geological Disaster in Qingling—Bashan Mountains. *Res. Soil Water Conserv.* **2005**, *12*, 240–243.
3. Wang, C.H.; Zhao, Y.J.; Bai, L.B.; Gou, W.; Meng, Q. Landslide Displacement Prediction Method Based on GA-Elman Model. *Appl. Sci.* **2021**, *11*, 11030. [[CrossRef](#)]
4. Miao, F.S.; Wu, Y.P.; Xie, Y.H.; Li, Y.N. Prediction of landslide displacement with step-like behavior based on multialgorithm optimization and a support vector regression model. *Landslides* **2018**, *15*, 475–488. [[CrossRef](#)]
5. Xie, H.L.; Zhang, L.; Lim, C.P. Evolving CNN-LSTM Models for Time Series Prediction Using Enhanced Grey Wolf Optimizer. *IEEE Access* **2020**, *8*, 161519–161541. [[CrossRef](#)]
6. Ma, Z.J.; Mei, G. Deep learning for geological hazards analysis: Data, models, applications, and opportunities. *Earth-Sci. Rev.* **2021**, *223*, 103858. [[CrossRef](#)]
7. Lian, C.; Zeng, Z.G.; Yao, W.; Tang, H.M. Multiple neural networks switched prediction for landslide displacement. *Eng. Geol.* **2015**, *186*, 91–99. [[CrossRef](#)]
8. Yin, S.D.; Feng, X.T.; Zhou, H.; Zhao, H.B.; Li, S.J. Study on GA-NN model for forecasting the displacement of landslides affected by rainfall. *Rock Soil Mech.* **2003**, *24*, 1038–1041.
9. Wang, C.H.; Zhao, Y.J.; Bai, L.B.; Guo, W.; Meng, Q.J. Application of renewal gray GM (1,1) model to prediction of landslide deformation with two case studies. *Hydrogeol. Eng. Geol.* **2009**, *36*, 108–111.
10. Deng, D.M.; Liang, Y.; Wang, L.Q.; Wang, C.S.; Zhang, Z.H.; Wang, C.; Dong, M.M. Displacement prediction method based on ensemble empirical mode decomposition and support vector machine regression—A case of landslides in Three Gorges Reservoir area. *Rock Soil Mech.* **2017**, *38*, 3660–3669.
11. Liu, Y.; Liu, D.; Qin, Z.M.; Liu, F.B.; Liu, L.B. Rainfall data feature extraction and its verification in displacement prediction of Baishuihe landslide in China. *Bull. Eng. Geol. Environ.* **2016**, *75*, 897–907. [[CrossRef](#)]
12. Pei, H.F.; Meng, F.H.; Zhu, H.H. Landslide displacement prediction based on a novel hybrid model and convolutional neural network considering time-varying factors. *Bull. Eng. Geol. Environ.* **2021**, *80*, 7403–7422. [[CrossRef](#)]
13. Jia, W.J.; Wen, T.; Li, D.C.; Guo, W.; Quan, Z.; Wang, Y.H.; Huang, D.X.; Hu, M.Y. Landslide Displacement Prediction of Shuping Landslide Combining PSO and LSSVM Model. *Water* **2023**, *15*, 612. [[CrossRef](#)]
14. Deng, L.Z.; Smith, A.; Dixon, N.; Yuan, H.Y. Machine learning prediction of landslide deformation behaviour using acoustic emission and rainfall measurements. *Eng. Geol.* **2021**, *293*, 106315. [[CrossRef](#)]
15. Yang, Z.R.; Xi, W.F.; Yang, Z.Q.; Shi, Z.T.; Huang, G.C.; Guo, J.Q.; Yang, D.Q. Time-Lag Response of Landslide to Reservoir Water Level Fluctuations during the Storage Period: A Case Study of Baihetan Reservoir. *Water* **2023**, *15*, 2732. [[CrossRef](#)]
16. Song, K.; Han, L.Y.; Ruan, D.; Li, H.; Ma, B.H. Stability Prediction of Rainfall-Induced Shallow Landslides: A Case Study of Mountainous Area in China. *Water* **2023**, *15*, 2938. [[CrossRef](#)]
17. Li, D.Y.; Sun, Y.Q.; Yin, K.L.; Miao, F.S.; Glade, T.; Leo, C. Displacement characteristics and prediction of Baishuihe landslide in the Three Gorges Reservoir. *J. Mt. Sci.* **2019**, *16*, 2203–2214. [[CrossRef](#)]
18. Wang, J.; Nie, G.G.; Xue, C.H. Landslide displacement prediction based on time series analysis and data assimilation with hydrological factors. *Arab. J. Geosci.* **2020**, *13*, 460. [[CrossRef](#)]
19. Meng, Q.X.; Wang, H.L.; He, M.J.; Gu, J.J.; Qi, J.; Yang, L.L. Displacement prediction of water-induced landslides using a recurrent deep learning model. *Eur. J. Environ. Civ. Eng.* **2020**, *27*, 2460–2474. [[CrossRef](#)]
20. Varnes, D.J. *Slope Movement Types and Processes*; Transportation Research Board Special Report; National Academy of Sciences: Washington, DC, USA, 1978.
21. Liu, G.R.; Chu, Z.C.; Guo, X.Z.; Liu, Y. Summary of main achievements of study on important geological and seismological problems in sanxia gorges of changjiang river. *Chin. J. Geol. Hazard Control* **1992**, *3*, 9–16.
22. Zhang, Z.Y.; Wang, S.T.; Wang, L.S.; Huang, R.Q. *Principles of Engineering Geological Analysis*; Geology Press: Beijing, China, 2009.

23. Yan, T.Z. *Hydrologic Engineering Geology and Environmental Protection*; China University of Geosciences Press: Beijing, China, 1994.
24. Liu, G.R.; Yan, E.C.; Lian, C. Discussion on classification of landslides. *J. Eng. Geol.* **2002**, *10*, 339–342.
25. Yan, E.C.; Liu, G.R. Discussion on the essential geological model for landslide. *J. Eng. Geol.* **2004**, *12*, 21–24.
26. Ma, Z.L.; Mei, G.; Piccialli, F. Machine learning for landslides prevention: A survey. *Neural Comput. Appl.* **2020**, *33*, 10881–10907. [[CrossRef](#)]
27. Chen, T.; Guestrin, C. XGBoost: A Scalable Tree Boosting System. In Proceedings of the 22nd ACM SIGKDD International Conference on Knowledge Discovery and Data Mining, San Francisco, CA, USA, 13–17 August 2016.
28. Zhang, K.; Zhang, K.; Cai, C.X.; Liu, W.L.; Xie, J.B. Displacement prediction of step-like landslides based on feature optimization and VMD-Bi-LSTM: A case study of the Bazimen and Baishuihe landslides in the Three Gorges, China. *Bull. Eng. Geol. Environ.* **2021**, *80*, 8481–8502. [[CrossRef](#)]
29. Bengio, Y.; Simard, P.; Frasconi, P. Learning long-term dependencies with gradient descent is difficult. *IEEE Trans. Neural Netw.* **1994**, *5*, 157–166. [[CrossRef](#)] [[PubMed](#)]
30. Yang, B.B.; Yin, K.L.; Lacasse, S.; Liu, Z.Q. Time series analysis and long short-term memory neural network to predict landslide displacement. *Landslides* **2019**, *16*, 677–694. [[CrossRef](#)]
31. Yan, L.; Chen, C.W.; Hang, T.T.; Hu, Y.C. A stream prediction model based on attention-LSTM. *Earth Sci. Inform.* **2021**, *14*, 723–733. [[CrossRef](#)]
32. Xu, J.C.; Jiang, Y.; Yang, C.B. Landslide Displacement Prediction during the Sliding Process Using XGBoost, SVR and RNNs. *Appl. Sci.* **2022**, *12*, 6056. [[CrossRef](#)]
33. Hochreiter, S.; Schmidhuber, J. Long Short-Term Memory. *Neural Comput.* **1997**, *9*, 1735–1780. [[CrossRef](#)]
34. Conte, E.; Pugliese, L.; Troncone, A. A Simple Method for Predicting Rainfall-Induced Shallow Landslides. *J. Geotech. Geoenviron. Eng.* **2022**, *148*, 4022079. [[CrossRef](#)]
35. Shrestha, S.; Pradhan, P.; Shrestha, H. Assessment of Rainfall-Induced Shallow Landslides in Kavre District, Nepal. *SCITECH Nepal* **2023**, *17*, 84–90. [[CrossRef](#)]
36. Mandal, P.; Sarkar, S. Estimation of rainfall threshold for the early warning of shallow landslides along National Highway-10 in Darjeeling Himalayas. *Nat. Hazards* **2021**, *105*, 2455–2480. [[CrossRef](#)]
37. Troncone, A.; Pugliese, L.; Lamanna, G.; Conte, E. Prediction of rainfall-induced landslide movements in the presence of stabilizing piles. *Eng. Geol.* **2021**, *288*, 106143. [[CrossRef](#)]
38. Huang, J.; Ju, N.P.; He, C.Y.; Xiao, Y. Establishment of early geohazard warning system using modern information technology. *J. Eng. Geol.* **2015**, *23*, 140–147.
39. Zhao, W.Y.; Ma, J.; Xiao, C.Y.; Pang, X. An Comprehensive Intelligent Rainfall-Deformation Warning Method for Rainfall-Induced Landslides. *Geogr. Geo-Inf. Sci.* **2022**, *38*, 17–22.
40. Xiao, T.; Zhang, L.M. Data-driven landslide forecasting: Methods, data completeness, and real-time warning. *Eng. Geol.* **2023**, *317*, 107068. [[CrossRef](#)]
41. Souza, F.T.D.; Ebecken, N.F.F. A Data Mining Approach To Landslide Prediction. *WIT Trans. Inf. Commun. Technol.* **2004**, *33*, 10.
42. Wang, C.H.; Guo, W.; Yang, K.; Wang, X.; Meng, Q.J. Real-Time Monitoring System of Landslide Based on LoRa Architecture. *Front. Earth Sci.* **2022**, *10*, 899509. [[CrossRef](#)]
43. Lin, Q.Y.; Yang, Z.P.; Huang, J.; Deng, J.; Chen, L.; Zhang, Y.R. A Landslide Displacement Prediction Model Based on the ICEEMDAN Method and the TCN-BiLSTM Combined Neural Network. *Water* **2023**, *15*, 4247. [[CrossRef](#)]
44. Zhang, Y.G.; Tang, J.; Cheng, Y.; Huang, L.; Guo, F.; Yin, X.J.; Li, N. Prediction of landslide displacement with dynamic features using intelligent approaches. *Int. J. Min. Sci. Technol.* **2022**, *32*, 539–549. [[CrossRef](#)]

Disclaimer/Publisher’s Note: The statements, opinions and data contained in all publications are solely those of the individual author(s) and contributor(s) and not of MDPI and/or the editor(s). MDPI and/or the editor(s) disclaim responsibility for any injury to people or property resulting from any ideas, methods, instructions or products referred to in the content.